An experimental and numerical study on the in-plane axial and shear behavior of sprayed in-situ concrete sandwich panels

An experimental and numerical study on the in-plane axial and shear behavior of sprayed in-situ concrete sandwich panels

M. Serpilli, F. Clementi and S. Lenci
Department of Civil and Building Engineering, and Architecture
Università Politecnica delle Marche, Italy
e-mail: m.serpilli@univpm.it

Abstract. The paper deals with the experimental and numerical characterization of the in-plane axial and shear mechanical behavior of sprayed in-situ reinforced concrete (RC) sandwich panels, used as structural walls. Axial compression tests were carried out on specimens with different slenderness ratios to study their behavior under axial vertical loads. While the diagonal compression test and shear load with constant compression test were respectively performed on squared panels, analyzing their response to in-plane horizontal lateral forces. Ultimate axial and shear loads have been experimentally determined and the most significant load-displacement diagrams have been reported. The obtained results have been compared with other experimental campaigns on RC sandwich panels and with conventional RC walls equations, available in codes of practice and literature. The structural potentialities of RC sandwich panels as load-bearing and shear walls are highlighted. The experimental investigation is corroborated by a 3D nonlinear finite element (FE) numerical analysis, considering the influence of the insulation layer, the efficiency of steel connectors, and the involved material nonlinearities.

1. Introduction

In the last decades, the use of sandwich panels in the construction field has intensively spread worldwide. Sandwich panels present the majority of advantageous features of the usual precast concrete wall panels, such as durability, fire resistance, structural and energy performance, costs, and use as shear walls, bearing walls, and retaining walls (see [1]–[3]). The most common and well-known building system based on precast RC sandwich panels usually involves complex construction and transportation steps. Therefore, in recent years, the use of cast in-situ (or sprayed in-situ) sandwich panels has started taking hold, due to the fast mounting procedures and relevant facilitation of the construction processes. The present research work will deal with sprayed in-situ RC sandwich panels.

Sandwich panels are made of a rigid and lightweight prefabricated insulation layer (e.g., expanded and extruded polystyrene, rigid polyurethane foam) between two wythes made of sprayed concrete (also known as shotcrete), reinforced by two galvanized steel welded meshes. The metallic meshes are connected through shear connectors (e.g., wire trusses, solid ribs of concrete, flat sleeve anchors, fiber composite rectangles, and small-diameter bent or welded bars), which enable the transfer of the in-plane shear forces between the two external layers. Shear connectors guarantee a composite or partially composite structural behavior, meaning that the whole panel acts totally or to some extent as a single unit under the applied loads [1]. Once in place, the sandwich wall panels provide the dual function of load carrying capacity and insulation. Fig. 1 shows some of the production and mounting procedures of sprayed in-situ RC sandwich panels. Concerning the spraying technique, the concrete is applied to the steel-reinforced insulation layer by a plastering machine (for mortars with granulometry from 3 to 8 mm). The shotcrete involves pumping of ready-mixed concrete to the nozzle: compressed air is introduced at the nozzle to impel the mixture onto the receiving surface. The spraying procedure must be made in successive steps, gradually adding shotcrete layers (max 20mm

thick) in order not to overcharge the concrete final product (see Fig. 2). Finally, the concrete wythe is leveled using a straight edge and, after 15/20 days, a mineral smoothing fibered plaster finish is applied.

Figure 1. Production and mounting procedures for sprayed in-situ RC sandwich panels

Figure 2. Spraying technique procedure

Several research and technical papers have been devoted to the study of the structural behavior of precast RC sandwich panels under axial, in-plane shear, and flexural loadings (see [4]–[6], for an extensive overview). The mechanical behavior of precast RC sandwich panels, under axial and eccentric compression loads, has been investigated in numerous research works, [7]–[15], employing axial compression tests. These studies mostly focused on the following experimental aspects: i) the load/deflection behavior; ii) the efficiency of the shear connectors (mainly, truss connectors or welded steel wires), providing composite or semi-composite panel behaviors; iii) the influence of the wall slenderness ratio H/t (H= height, t= thickness) on the ultimate load and possible buckling phenomena; iv) the influence of the vertical steel ratio on the ultimate load. The experimental results revealed that the ultimate compressive strength of the panels decreases nonlinearly with the increase of the slenderness ratio and increases almost linearly with the increase of the vertical steel. The presence of an initial eccentricity of the applied compression load entailed a reduction of the ultimate failure load, due to the appearance of out-of-plane buckling. Moreover, while the majority of previous papers [7]–[11] developed 2D simplified nonlinear FEM models to reproduce the experimental data, very few works can be found on the 3D nonlinear FEM design, taking also into account the influence of a rigid insulation layer, [12], [16]. As far as the in-plane shear under a constant compression load of RC sandwich panels is concerned, most of the research work accomplished up to date was focused upon the experimental characterization of the seismic behavior after a certain number of horizontal lateral loading cycles, [17]–[25]. Precast and cast in-situ RC sandwich walls were tested through shear tests with/without constant compression. Boundary element type, aspect ratio H/L (L=length), horizontal reinforcement ratio, concrete compressive strength, and level of axial load were considered as test parameters. The experimental results in terms of stiffness, shear strength, ductility, and energy dissipation showed high values of the maximum horizontal load applied to the structural systems, residual bearing capacity for vertical loads. The seismic performances of the tested sandwich panels were comparable with those of common RC panels. The flexural behavior of precast RC sandwich panels and, thus, their possible use as slabs, was experimentally and theoretically studied, considering the influence of shear connectors on the composite action and the failure mechanism, see [26]–[34]. The main findings showed that the type and the arrangement of connectors played a key role in the composite behavior of panels: for instance, truss girder and inclined (steel, FRP, CFRP, GFRP, etc.) connectors provided a high degree of composite action, while wired connectors orthogonal to the concrete wythes were not able to transfer shear loads, resulting in a semi-composite behavior.

In view of the above, a limited number of researches can be found in literature about the experimental characterization of the in-plane structural (axial and shear) behavior of sprayed (cast) in-situ sandwich panels. For this reason, further investigations from the experimental of view are needed to thoroughly exploit their structural potentialities as bearing walls or shear walls. Moreover, the construction of a reliable 3D nonlinear FEM model is essential to support the experimental results and to fully validate the RC sandwich panel mechanical behavior. The use of a 3D numerical model, instead of simplified 2D FEM models, allows highlighting the influence on the structural response of the sandwich panel constituents (concrete wythes, steel connectors, vertical and horizontal steel meshes, EPS layer).

The present paper is aimed at studying the experimental and numerical in-plane axial and shear mechanical performances of sprayed in-situ RC sandwich panels. The tested sandwich panels are characterized by orthogonal wired steel connectors joining the concrete layers. Concerning the experimental campaign, axial compression tests have been performed to assess the structural performance of squat and slender panels as load-bearing walls. While diagonal compression tests and shear tests with constant compression on squared panels have been carried out to study the mechanical behavior under horizontal forces, considering also the influence of vertical loads. The results of shear tests allowed measuring the diagonal tensile (shear) strength of RC sandwich panels and evaluating their seismic lateral response as shear walls. The obtained experimental results, in terms of ultimate

loads and strengths, have been compared to other experimental programs on similar RC sandwich panels and conventional RC walls equations, available in codes of practice and literature. The experimental investigation is corroborated by a 3D nonlinear FEM numerical analysis, simulating the aforementioned tests. The FEM solid model takes into account the influence of the insulation layer, the efficiency of steel connectors in the composite action, and the involved material nonlinearities.

2. Experimental program

The experimental campaign was carried out on sandwich panels, consisted of a sheet of an insulation material, namely Expanded Polystyrene (EPS), reinforced by two steel meshes connected by steel connectors. The EPS sheet of thickness 140 mm had straight profiles and density of 22 kg/m^3. The galvanized welded steel meshes were made of ϕ5 wires (with 100mm vertical bar spacing and 75mm horizontal bar spacing), connected at the top and bottom by welded ϕ8/15 U-shaped steel bars. Moreover, the two steel meshes are linked together with galvanized wires having diameter of 3 mm, welded orthogonally to the meshes and EPS layer in quantity of 20 per m^2. The panels were finally sprayed on both side with two 50 mm-thick concrete layers. The total thickness of the panel is of 240 mm.

The experimental program has been carried out at the "Laboratorio Prove Materiali Strutture", DICEA, Università Politecnica delle Marche, and consisted of the following tests:

1. Axial compression test
2. Diagonal compression test
3. Shear test with constant compression.

2.1 Materials and test specimens

The company, supplying the RC sandwich panels specimen for the experimental campaign, provided all the information regarding the composition, mixture ratio, and mechanical properties of the sprayed concrete. A ready-mixed concrete, with sand no greater than 3 mm and specific additives to improve adhesion and workability, was employed. The main material characteristics are reported in Table 1.

Table 1
Sprayed concrete and steel material properties

Relative density of powder	1425 kg/m^3
Mortar density	2080 kg/m^3
Granulometry	< 3 mm
Water content	18%
Characteristic cube strength f_c (EN 1015-11)	30 MPa
Mean cube strength f_{cm} (EN 1015-11)	> 35 MPa
Characteristic cylindric strength f_c' (EN 1015-11)	25 MPa
Elastic moduli (28 days)	> 39000 MPa
Chloride content	< 0.1%
Characteristic steel yield strength f_y	450 MPa

The experimental tests were performed on twelve panels: three for diagonal compression tests, six for axial compression tests and three for shear tests with compression. Two types of panels were tested, varying their total heights and, thus, their aspect H/L and slenderness H/t ratio, respectively. In the sequel, squat panels presented an aspect ratio H/L ≤ 1; while slender panels had an aspect ratio H/L ≥ 2. All the geometrical details and test designations are presented in Table 2.

Table 2
Test specimens, dimensions, aspect ratio and slenderness ratio

Test	N. Specimens	H (mm)	L (mm)	t (mm)	H/B	H/t
Diagonal Compression (CD)	3	1100	1100	240	1	4.6
Axial Compression (CC)	3	1100	1100	240	1	4.6
Axial Compression (Cc)	3	3000	1100	240	2.7	12.5
Shear with Compression (PT)	3	1100	1100	240	1	4.6

Two reinforced concrete beams were built at the top and bottom of all panels, tested at axial compression, and horizontal shear with constant compression. The RC beams were designed to avoid stress concentration, to enhance a better internal distribution of the loads, and to facilitate transport and handling operations (see Fig. 3). The upper and lower RC beams were connected to the concrete wythes and steel mesh by welded ϕ8/15 U-shaped steel bars.

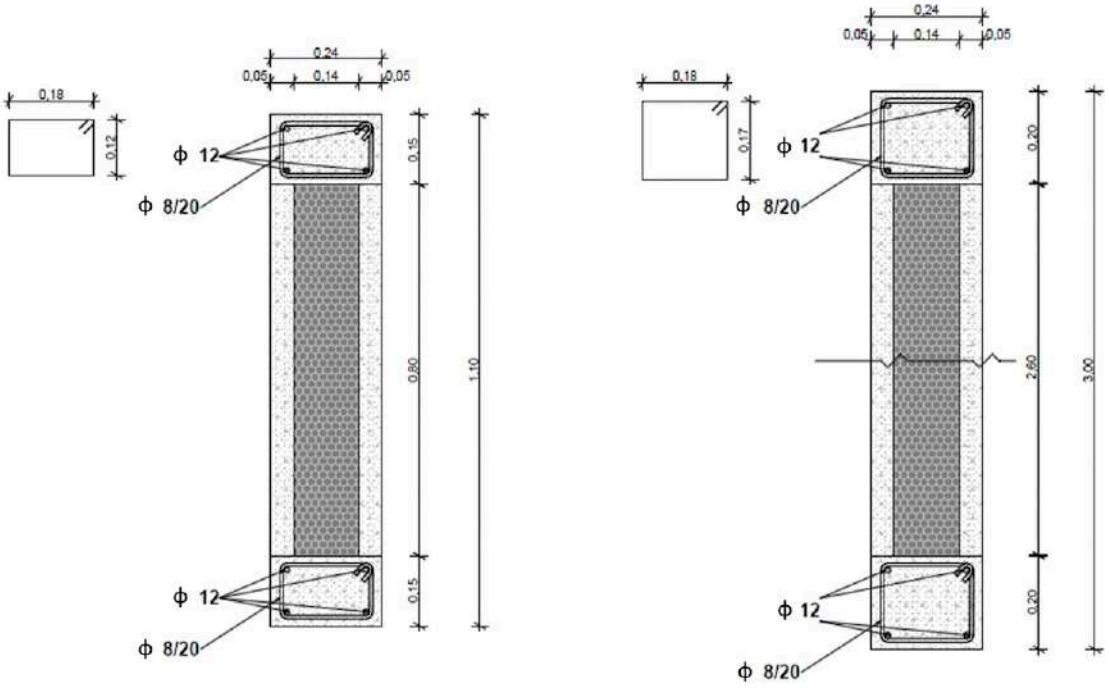

Figure 3. Technical drawings of the concrete sadwich panels for axial and eccentric compression tests.

To ensure correct execution of the diagonal compression test and avoiding stress concentration at the loading areas, two triangular concrete regions with a frettage (metallic mesh ϕ5 20/20) were built in correspondence of the specimen corners (see Fig. 4). The full concrete casting areas have been designed for a better distribution of the compression load within the two concrete wythes. The corresponding stress state induces the panel failure when the principal tensile stress at its center attains its maximum value.

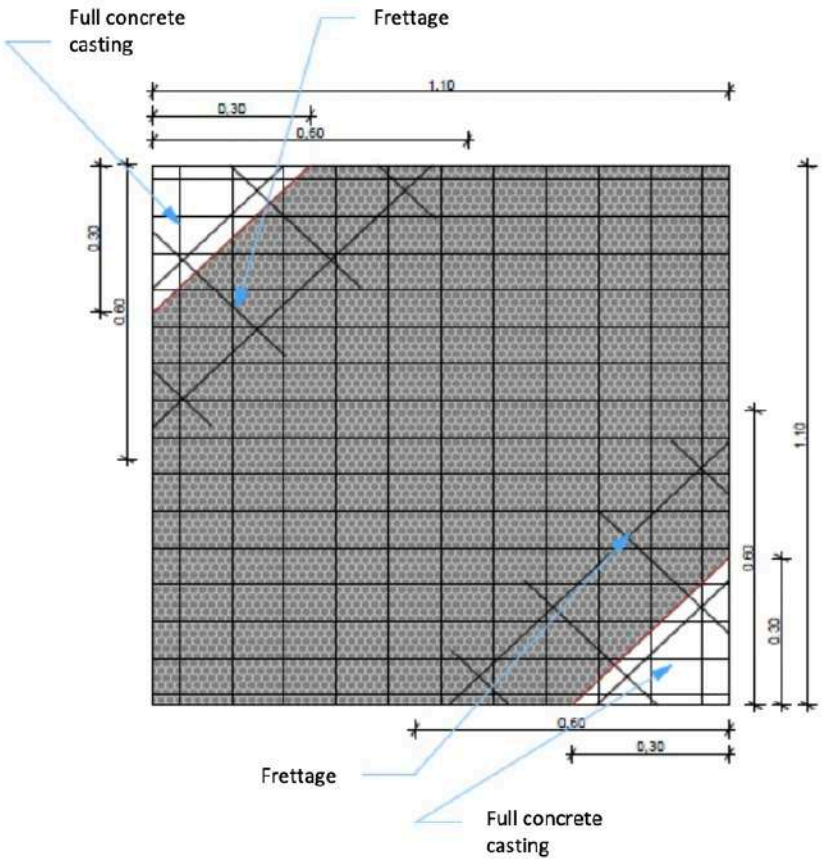

Figure 4. Technical drawings of the concrete sandwich panels for diagonal compression tests.

2.2 Test setup and instrumentation

Fig. 5 shows the configuration of the test apparatus for the axial compression tests for the rectangular specimens (1100 mm x 3000 mm). The test set up for the squat panels (1100 mm x 1100 mm) was substantially similar. The sandwich panels were placed vertically, restrained on top. The load was applied by means of four hydraulic jacks (max. load 500 kN), fixed to the reaction frame. The hydraulic jacks were connected to a hydraulic control unit with a pressure transducer, enabling the measurement of the applied force. As regards the axial compression test, the load was applied following the panel mid-plane. A thick steel plate was interposed between the hydraulic jacks and the panels top end in order to ensure a uniform distribution of the load. Each panel was instrumented by two transducers LVTD (S_{vf} and S_{vb}), measuring the vertical displacements. To measure the out-of-plane lateral deflection, three transducers (S_1, S_2, and S_3) were placed orthogonally to the specimen plane at 1/4, 1/2 e 3/4 of the panel height. For squat panels (1100 mm x 1100 mm), just a horizontal transducer was placed at ½ of the height. Finally, an LVTD (S_4) was placed across the thickness at half of their heights to measure the transversal separation displacement between the two concrete layers. All transducers had a $\pm 1 \times 10^{-3}$ mm sensibility and worked over a base length of 30 mm, for 1100 mm x 1100 mm panels, and over 100 mm, for 1100 mm x 3000 mm panels, respectively.

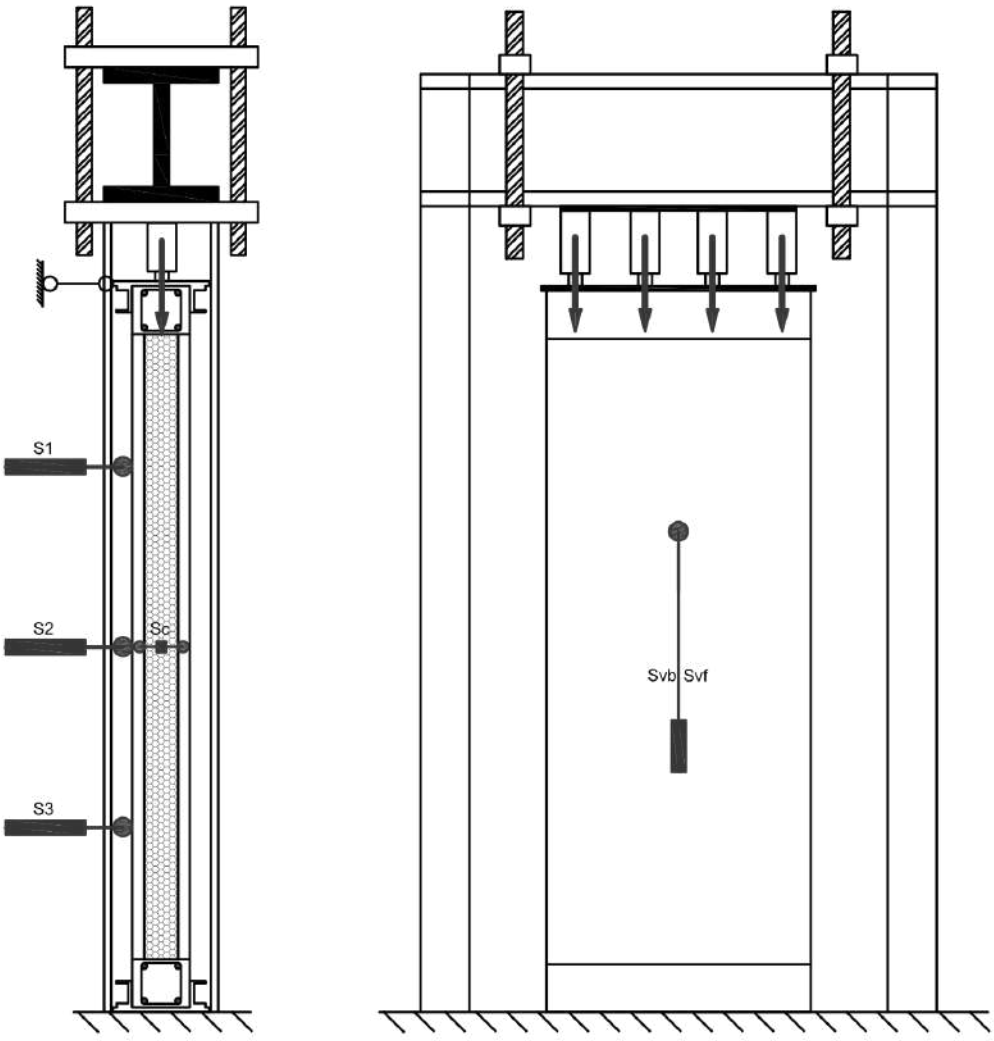

Figure 5. Test apparatus for axial compression tests: lateral and front views

Since reference standards for testing RC sandwich panels under diagonal compression are lacking, a testing procedure specifically developed for masonry walls (ASTM E519/E519M-15, [35]) was used and adapted to the specific case, (see, e.g., [9]). Fig. 6a shows the test set up for the diagonal compression test, which was carried out using a slide pushed by six hydraulic jacks (max. load 500 kN). The panels were placed at a 45° angle of rotation between the bottom slide and the reaction frame. To avoid stress concentration, two L-shape profiles were placed at the top and bottom corners. In this case, the instrumentation consisted of a pressure transducer, for the applied load measurement, and on four displacement transducers, working in a range of ±50 mm, located vertically (S_{vf} and S_{vb}) and horizontally (S_{of} and S_{ob}), to measure the strains with a gauge length of 600 mm.

Finally, Fig. 6b shows the test set up for shear tests with a constant compression load, adapting the experimental guidelines provided in [36], [37]. The test configuration was similar to the axial compression set up. A compression load of 400 kN, corresponding to a level axial load ratio $N/(A_g f_c)\%=12\%$, was applied at the top end using four hydraulic jacks (max. load 500 kN) and kept constant throughout the whole test. The horizontal force F_h was applied by means of an additional hydraulic jack (max. load 500 kN) through an L-shaped steel profile. The horizontal displacements of the panel top end were measured thanks to a horizontal LVTD (S_o). Moreover, two diagonal transducers (S_{d1} and S_{d2}), working in a range of ±50 mm, were placed in the center of the panel in an extensometric configuration to measure strain over a base length of 500 mm.

All LVTDs registered positive values in contraction and negative values in the case of elongation.

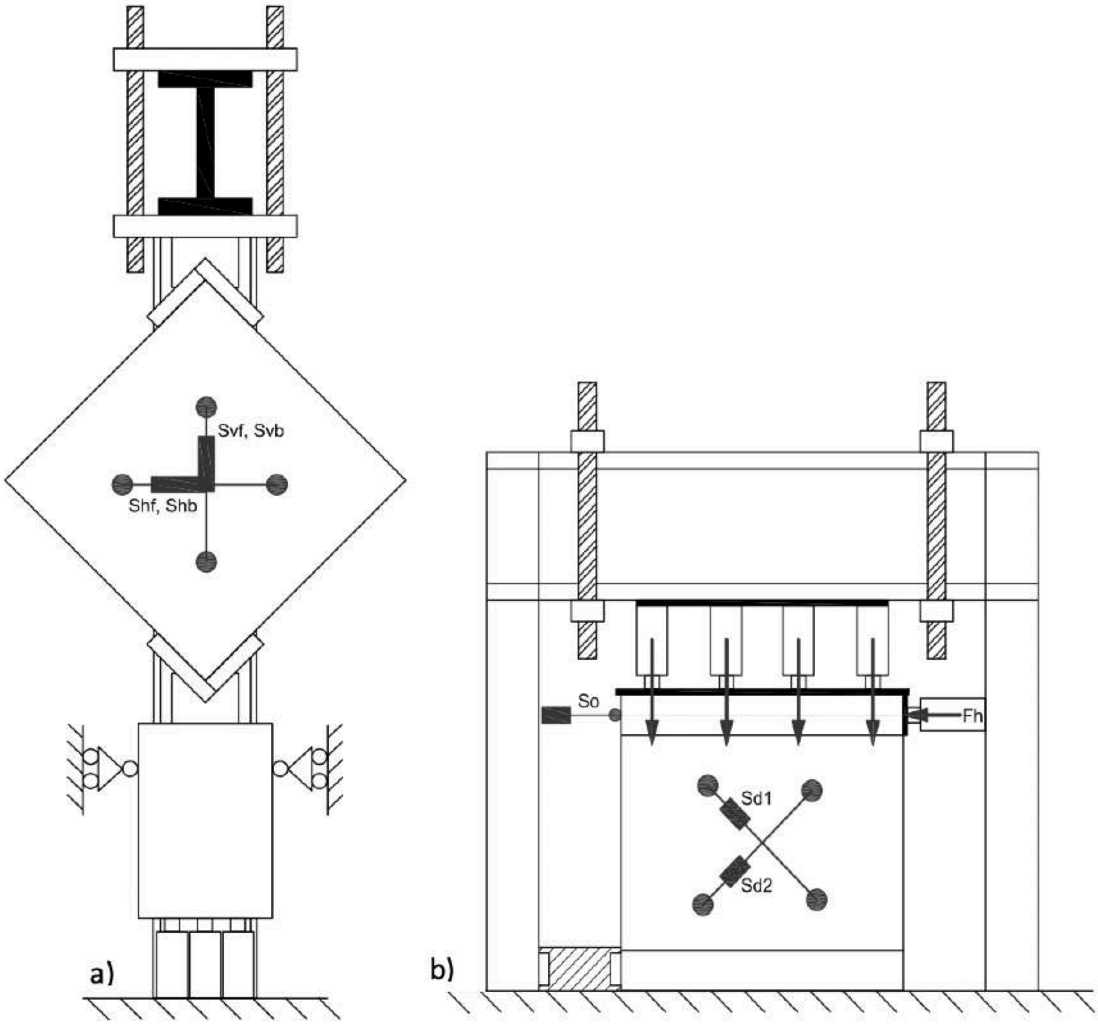

Figure 6. Test set ups for a) diagonal compression test and b) shear test with compression

3. Experimental test results

The present section is devoted to the description of the main experimental results, showing the load deflection curves, ultimate loads and lateral deflection curves.

3.1 Axial compression test results

The axial compression tests were carried out on four squat panels (1100 mm x 1100 mm) and on three slender panels (1100 mm x 3000 mm), respectively.

- **Squat panels (1100 mm x 1100 mm)**

Fig. 7 depicts the load versus the vertical displacements diagram: the displacements were recorded by LVTDs on the front side (continuous line) and the backside (dotted line) of the three tested specimens. The load-displacement trends showed a linear relationship, ending after the appearance of the first crack on the surface of the concrete. After increasing the load, the vertical displacement nonlinearly increased due to the evolution of the cracking phenomenon till the complete rupture of the panel. A slight change in slope between the front and back LVTDs curves, registered for specimen

CC1, is attributed to the occurrence of the first crack. The front side LVTD monitored the displacements of the concrete wythe, in which the first crack appeared, and, thus, its associated curve presented a minor slope. The formation of the first crack produced a stress reduction in the front wythe, and a consequent stress increase on the other back wythe. Similar results have been obtained in [15]. The significant deviations in slope of the curves associated with specimens CC2 (back LVTD, blue dotted line) and CC3 (front LVTD, green continuous line) were mainly caused by two factors: on the one hand, the first crack appearance in one wythe affected the load distribution on the other concrete layer, resulting in a stiffness reduction and, hence, a lower slope; on the other hand, the more pronounced separation between the front and back LVTDs curves could also be due to material or geometrical imperfections, classically associated with non-homogeneous concrete curing and drying and with the industrial spraying technique.

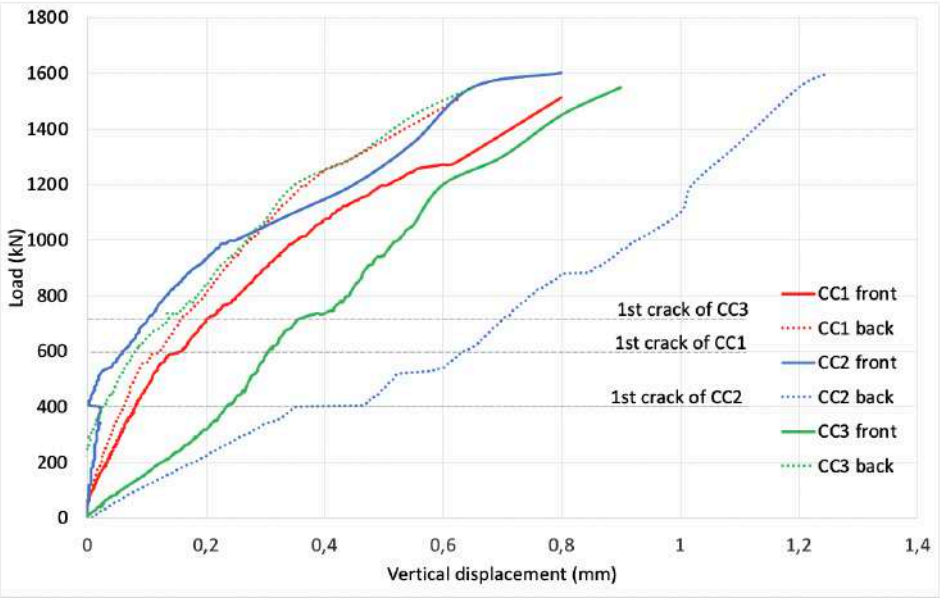

Figure 7. Load-vertical displacement diagram for 1100 mm x 1100 mm panel

The horizontal separation between the concrete wythes is reported in Fig. 8a. The separation displacement was negligible for squat panels, being less than one millimeter. The load vs lateral deflection plot is reported in Fig. 8b. This particular displacement remained, in general, quite small and without significant variations under increasing loading up to failure: indeed, concerning squat panels, the effect of buckling of the concrete layers and the whole sandwich panel cannot be considered relevant and did not influence the failure mechanisms. The in-ward inversion of the horizontal displacement evolution in correspondence of the first crack (about 400kN) for panel CC2 could have been caused by a local instability of just one of the concrete layers.

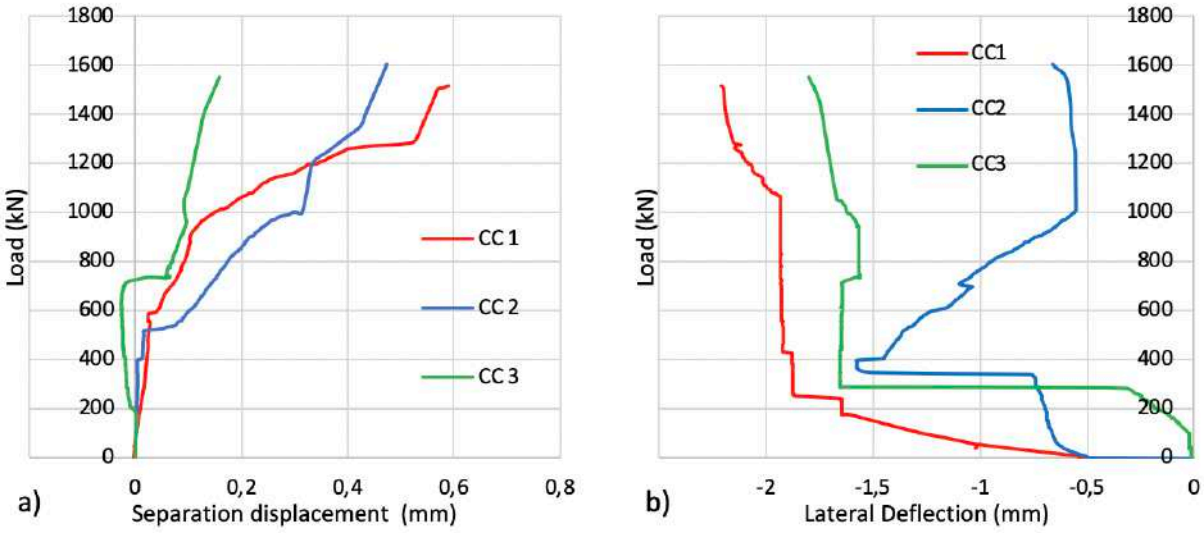

Figure 8. Axial compression test: a) Load-separation displacement diagram and b) load-lateral deflection diagram

The cracking pattern was marked on each face of the tested specimens. The failure occurred as a result of concrete crushing due to compression, characterized by the classical vertical cracks pattern (see Fig. 9a), and buckling of the metallic mesh close to the upper and/or lower reinforced beam (see Fig. 9b, c), with consequent concrete expulsion. No evident separation of the sprayed concrete was visible on the lateral sides of the specimens. The most evident concrete splitting from the insulation layer was registered in correspondence of the upper and lower areas, where the concrete cover was expelled.

Figure 9. Specimen after failure: a) concrete compression failure and crack pattern, b) and c) mesh failure

- **Slender panels (1100 mm x 3000 mm)**

The load-vertical displacement plot is reported in Fig. 10: as in the previous set-up for squat walls, the displacements were recorded by LVTDs on the front side (continuous line) and the backside (dotted line) of the three panels. All panels Cc1, Cc2 and Cc3 showed a linear behavior from the beginning of the test until the formation of the first crack. By increasing the load, the vertical displacement regularly increased until the overall trend became nonlinear and rupture occurred. The difference in terms of slope for the back and front LVTDs curves is attributed to the first crack formation, which produced a redistribution of the stresses between the two concrete wythes and led the crack and plastic yielding on one face (see [11], [15], for similar experimental results). Concerning specimens Cc1 and Cc3, the two concrete wythes initially behaved in the same way, with shortening deformations; in a second phase, one of the two concrete layers was characterized by a significant decrease of the shortening deformation due to the appearance of an out-of-plane buckling phenomenon. Slender panels behavior under compression are relevantly influenced by their slenderness ratio and undesired geometrical or load eccentricities, which could lead to bending behavior due to out-of-plane instabilities.

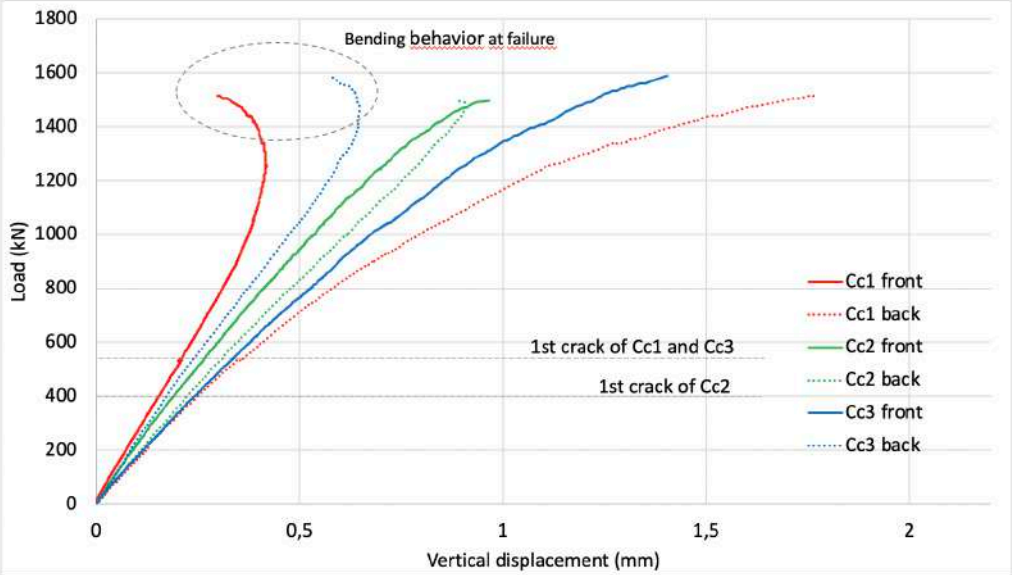

Figure 10. Load-vertical displacement diagram for 1100 mm x 3000 mm panels

The horizontal separation between the concrete layers is reported in Fig. 11a. As for the axial test of squat panels, the separation was far less than one millimeter and, thus, negligible. The load vs lateral deflection diagram is reported in Fig. 11b, considering the LTDV at mid-height of the panels. The plot shows that the lateral deflection linearly increases, reaching peaks of about 10 mm. Clearly, the strong increase in the out-of-plane displacements was caused by a buckling phenomenon, due to the slenderness of the specimens. In Fig. 12, the deformed shape of the slender panels is plotted at different load stages (400 kN, 800 kN, and 1200 kN), considering the displacements at ¼, ½, and ¾ of the panel height, registered by the LVTDs. This effect was evidently not registered for squat panels, in which instability phenomena are not prominent.

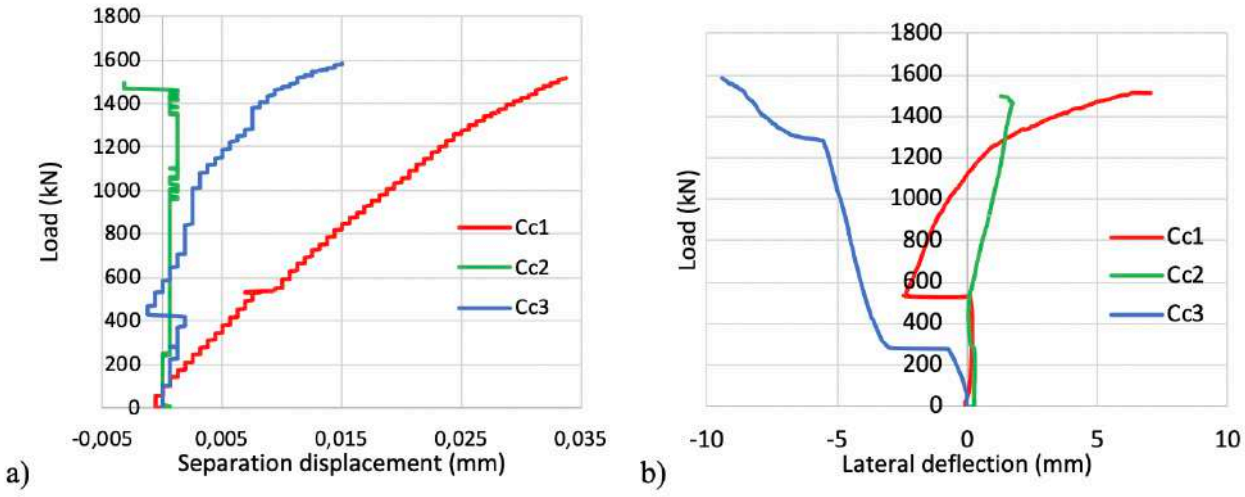

Figure 11. Axial compression test: a) Load-separation displacement diagram and b) load-lateral deflection diagram

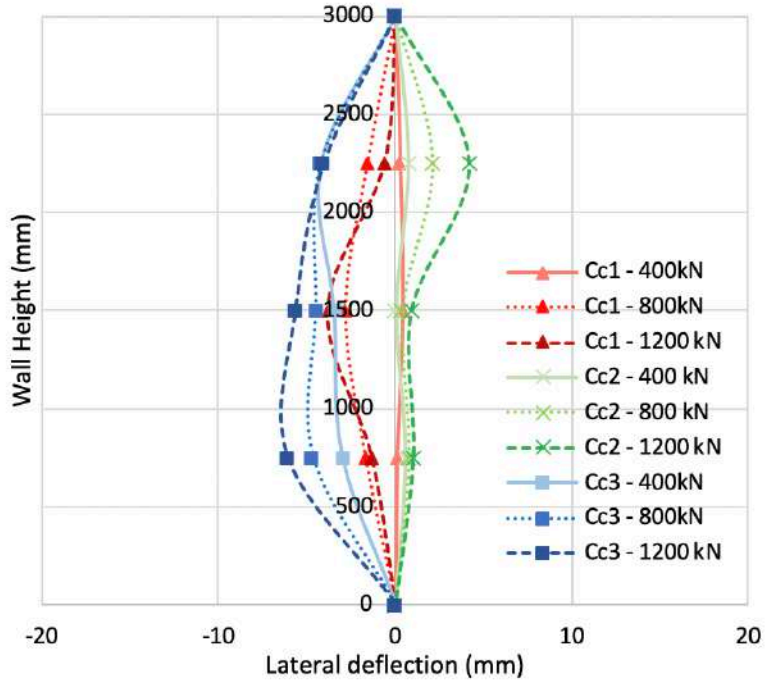

Figure 12. Lateral deflection at different load stages for slender panels

In the present case, the collapse occurred as a combination of out-of-plane buckling (see Fig. 13a), mostly due to the panel slenderness, and of concrete crushing modes at the top and bottom edges due to the high compressive loads (see Fig. 13b, c). The failure was sudden and violent for all specimens. The crack patterns mostly ran along the vertical direction with a relevant horizontal crack line at mid-height due to out-of-plane buckling. No evident separation of the sprayed concrete has been registered all along the panel length, as it is shown in Fig. 11a. The only concrete layer splitting from the EPS substrate was visible close to the top and bottom RC concrete beams, where the concrete crushed.

Figure 13. Specimen after failure: a) lateral buckling failure, b) and c) concrete beam failure

The maximum loads (Ultimate Load), reached in each axial test, are reported in Table 3, together with their mean value. It is interesting to notice that the Ultimate Load presented a slight decrease with the slenderness ratio H/t, which is coherent with other literature results (see, e.g., [7], [9], [11]). The maximum load for squat panels is about 1.5% higher than the load of the slender panels.

Table 3
Axial compression test: Ultimate Loads

Test	H/L	Ultimate Load (kN)
CC1		1512
CC2	1	1550
CC3		1602
Mean Value		1555
Cc1		1515
Cc2	2.7	1495
Cc3		1588
Mean Value		1532

In what follows, the nominal compressive strengths values are compared with those obtained in [7] and [9], considering sandwich panels presenting similar slenderness ratio H/t. The nominal compressive strength σ_c is obtained by dividing the ultimate load by the gross concrete area. The main differences rely on the vertical (ρ_v) and horizontal (ρ_h) steel area ratios and the thickness of the concrete layers, as reported in Table 4. The horizontal steel ratio in RC walls has very little influence on the ultimate compressive strength (see [8]), hence, the axial compression capacity in sandwich

walls, in terms of ultimate load and compressive strength, is mainly influenced by the thickness of the concrete wythes and vertical steel area ratio. The value of ultimate axial loads depends also on the composite action of the sandwich panels, related to the efficiency of the shear connectors.

Table 4
Comparison of nominal compressive strength values of other experimental axial compression test

Test	H/t	ρ_v %	ρ_h %	$t_{concrete}$ (mm)	σ_c (MPa)
Present Research	12.5	0.40	0.54	50	13.9
Gara et al. (2012) [9]	12.7	0.27	0.25	35	11.2
Mugahed Amran et al. (2019) [11]	13.3	0.33	0.77	82.5	8.1

Finally, Table 5 presents a comparison of the experimental ultimate load values with the ultimate compressive load of RC walls (P_u), provided by scientific literature [8], [38], and code of practice [39]. It is worth noticing that all empirical formulae are very conservative, especially for high H/t values.

Table 5
Comparison of the experimental Ultimate Loads with empirical and code of practice values

Model	Equation	H/t	Ultimate Load (kN)
Present Research (experimental)	-	1	1555 (mean value)
		2.7	1532 (mean value)
ACI 318-14 [39]	$P_u = 0.55\phi f_c A_c \left[1 - \left(\frac{H}{32t}\right)^2\right]$	1	1244
		2.7	1076
Saheb et al. [38] H/B<2	$P_u = 0.55\phi\left[f_c A_c + (f_y - f_c)A_{sc}\right]\left[1 - \left(\frac{H}{32t}\right)^2\right] \times \left[1.2 - \left(\frac{H}{10B}\right)\right]$	1	1427
H/B>2	$P_u = 0.55\phi\left[f_c A_c + (f_y - f_c)A_{sc}\right]\left[1 - \left(\frac{H}{32t}\right)^2\right]$	2.7	1135
Benayoune et al. (2006) [8]	$P_u = 0.4\phi f_c A_c \left[1 - \left(\frac{H}{40t}\right)^2\right] + 0.67 f_y A_{sc}$	1	1405
		2.7	1321

$\phi = 0.7$, f_c= characteristic concrete cube strength = 30 N/mm^2, f_y= characteristic steel yield strength = 450 N/mm^2, A_c= gross concrete area, A_{sc}= steel area in compression. The values for f_c, f_y have been provided by TCS s.r.l.

3.2 Diagonal compression test results

The diagonal compression tests were carried out on three squat panels (1100 mm x 1100 mm). Fig. 14 reports the plot of the load versus vertical shortening/horizontal elongation for the panel CD1, measured by four LTDVs, on the front (S_{vf} and S_{of}) and back (S_{of} and S_{ob}) sides, respectively. The shear behavior showed a first linear branch until the first cracking, then a nonlinear behavior until the ultimate load is reached. At the first stage of loading, the average horizontal elongation was lower than the vertical shortening and became similar after concrete cracking. The sandwich panels did not exhibit a sudden fragile failure: the final collapse of the panel occurred after an extensive diffuse concrete cracking. The failure mechanism was characterized by two different rupture modes, namely, failure due to tensile stresses (a) and localized concrete crushing (b) on the corner (load application point), as shown in Fig. 15. The most significant result on the ultimate load was provided by specimen CD2, which is the only one presenting a more evident diagonal tensile failure. The specimens revealed an evident capacity of load distribution among their constituents thanks to the presence of the metallic mesh and steel connectors.

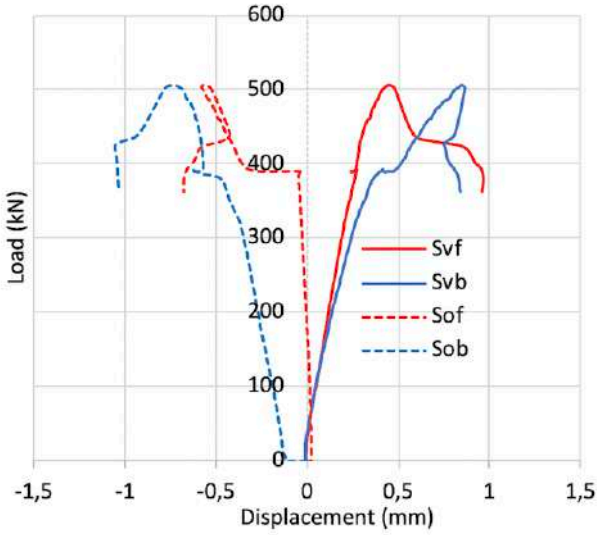

Figure 14. Diagonal compression test: vertical shortening and horizontal elongation of panel CD1

Figure 15. Diagonal compression test: crack patterns at failure

The shear strength in the center of the panel is obtained according to the procedures indicated in ASTM E519/E519M-15 [35]. The shear stress τ is calculated using an isotropic linearly elastic model, [40]:

$$\tau = \frac{0.707P}{A_n},$$

where P is the applied load, A_n is the net area of the specimen cross-section calculated according to the following equation:

$$A_n = \left(\frac{H+L}{2}\right) Bn^*,$$

where H, L, and B represent, respectively, the height, the width, and the total thickness of the specimen, and n^* is the percentage of the gross area of the unit that is solid, expressed as a decimal. The values of the ultimate loads, shear strengths, and the type of failure mode are reported in Table 6.

Table 6. Diagonal compression test: ultimate load, shear strength, and failure mode

Test	Ultimate Load (kN)	Shear strength (MPa)	Failure mode
CD1	505	3.24	a, b
CD2	465	2.99	a
CD3	479	3.07	a, b
Mean Value	446.4	3.10	

The shear strength values are in good agreement with the results obtained in [9] with similar RC sandwich panels under diagonal compression (mean shear strength value = 2.90 MPa).

3.3 Shear test with constant compression results

The shear tests with constant compression load were carried out on three squat panels (1100 mm x 1100 mm). All tests were conducted with a constant axial load of 400 kN.

The lateral load versus horizontal drift curves are displayed in Fig. 16. The drift was computed as the ratio between the measured lateral horizontal displacement and the panel height. The overall behavior can be considered linear, till a mean value of about 0.06% drift, corresponding to the appearance of the first diagonal cracks. The maximum strength for panel PT3 was reached at 0.13% drift and remained approximately constant till the ultimate drift at 0.29%. Panel PT3 behavior was characterized by an extended post-elastic region after the load peak value: in this case, the steel rebars reached the yielding threshold and the concrete crushing was delayed. Concerning specimens PT1 and PT2, the maximum strength was reached at 0.13% and 0.12% drifts, respectively, but it suddenly decreased as the drift increased. This rapid degradation of strength was likely due to the simultaneous steel yielding and concrete crushing, followed by the abrupt rupture by concrete spalling.

Fig. 17 shows the final cracking patterns, which have been highlighted in black color. The crack maps were mainly constituted by diagonal shear cracks, due to tension failure mode along the diagonal strut under compression. Besides, a relevant concrete spalling was visible on the opposite bottom corner with respect to the horizontal load application point, near the steel block used to prevent the possible panel sliding.

In Table 7, the values of the maximum shear load and maximum drift are listed. The failure maximum loads were coherent with the results obtained in [22], which analyzed the seismic behavior of sandwich concrete panels under cyclic loading.

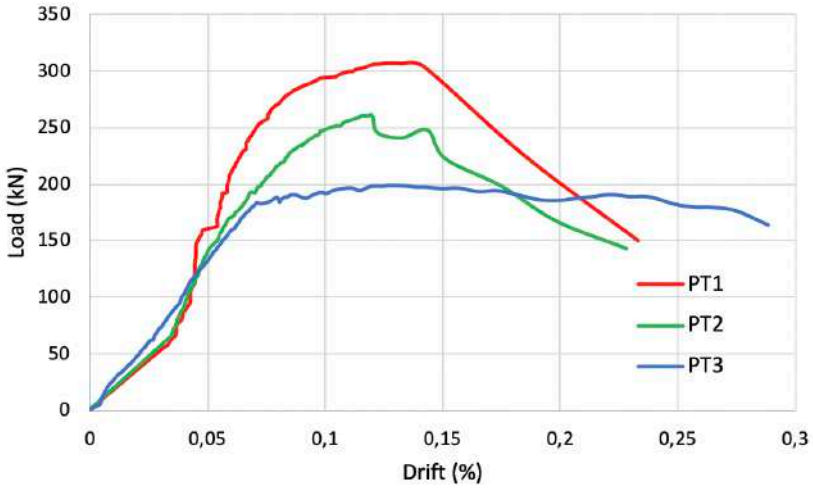

Figure 16. Lateral load-drift diagram for 1100 mm x 1100 m panels

Figure 17. Shear test with constant compression: crack patterns at failure

Table 7
Shear test with constant compression: max shear load, max drift

Test	Max shear load (kN)	Max drift (%)
PT1	307	0.23
PT2	261	0.23
PT3	200	0.29
Mean Values	256	0.25

Table 8 presents the predictive shear strength of the tested specimens using codes [39], [41], and literature empirical and semi-empirical equations [42]–[44]. All equations have been adapted to the present case of study. The shear strength $V_u = V_c + V_s$ is given by two contributions, namely, V_c, the shear strength provided by concrete, and V_s, the nominal shear strength provided by horizontal reinforcement. In order to apply the shear strength prediction formulae, which have been proposed for RC walls, the sandwich panels must satisfy the following features: i) the walls must have outer

concrete wythes with an inner EPS core; ii) the panels are without openings; iii) the specimens are tested under static loading; iv) the main failure mechanism is represented by diagonal tension shear or mixed flexural and shear. The sandwich panels satisfied the above characteristics.

The proposed provisions of ACI 318-14 ([39]) for predicting walls shear strength overestimated the shear strength of the tested walls, while Code EC8 ([41]) gives a closer prediction, with a ratio V_u/V_{exp} close to 1. Concerning the equations, provided by scientific literature, the best shear strength predictions were obtained using both Gulec and Whittaker [44] (V_u/V_{exp} =1.14) and Carrillo and Alcocer [43] (V_u/V_{exp} =0.99). The provision proposed by Carrillo and Alcocer [7] is more conservative and comparable with those proposed by EC8.

Table 8
Comparison of the experimental mean shear strength value with empirical and code of practice formulae

Model	V_c	V_s	Shear strength V_u (kN)	V_u/V_{exp}
Present Research (experimental)	-	-	256	-
ACI 318-14 [39] H/B<1.5	$V_c = 0.25\sqrt{f_c'}tL$	$V_s = \rho_h f_{yh} tL$	404	1.58
EC8 [41] $1.5N_{sd}/tBf_c' > 0.10$	$V_c = 0.15\sqrt{f_c'}tL$	$V_s = [\rho_h f_{yh}(M/VL - 0.3) + \rho_v f_{yv}(1.3 - M/VL)]$	278	1.09
Sanchéz-Alejandre and Alcocer (2010) [42]	$V_u = (\gamma\eta_v + P/A)\sqrt{f_c'} + \eta_h\rho_h f_{yh}$, $\gamma = 0.42 + 0.08\,M/VL$, $\eta_v = 0.75 + 0.05\rho_v f_{yv}$, $\eta_h = 1 - 0.16\rho_h f_{yh}$		342	1.33
Carrillo and Alcocer (2013) [43]	$V_u = \left(0.19\sqrt{f_c'} + 0.7\rho_h f_{yh}\right)A$		292	0.99
Gulec and Whittaker (2011) [44]	$V_u = \left(1.5\sqrt{f_c'}A + 0.25F_{vw} + 0.4P\right)/\sqrt{H/L}$		252	1.14

f_c'= characteristic concrete cylindric strength, f_{yv}= characteristic steel yield strength of vertical reinforcement, f_{yh}= characteristic steel yield strength of horizontal reinforcement, A= wall area, P = applied compression load, $M/VL = 1$, being $M = VH$ and $H/L = 1$.

4. Finite element analysis and numerical results

A FE model able to reproduce the data of the whole experimental campaign (axial compression, diagonal compression, shear with compression) was developed. The panels were modeled with solid tetrahedron elements with 4 nodes and linear shape function, and an optimized regular mesh was used for discretization. The nonlinear behavior of the concrete layers is represented by a Total Strain Crack Model (smeared approach) based on fixed stress–strain law concepts available in Midas FEA [45], while the steel rebars were modeled with 2-nodes links. In this way, the cracks are fixed in the direction of the principal strain vectors being unchanged during the loading of the structure. Perfect contact is assumed between concrete wythes and steel rebars. The compression behavior of the concrete was modeled by a constitutive law comprising a parabolic hardening rule and a parabolic softening branch after the peak of resistance, the tensile behavior was characterized by a linear hardening branch followed by a nonlinear softening branch [45] (Fig. 18). Moreover, the influence of the EPS layer has been taken into account in the simulations. The FE model was composed of 396 elements with 1875 DOFs. Mechanical properties of the materials were reported in Table 9: the characteristic concrete cubic strength and characteristic steel yield strength correspond to those values provided by the building company.

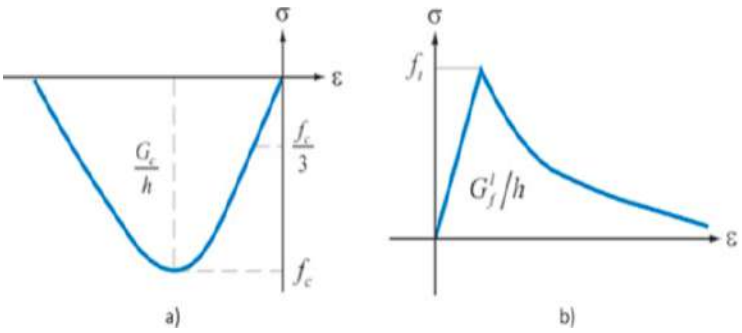

Figure 18. Compression and tension concrete behaviors (see Ref. [45])

Table 9
Material properties used in the FE model

Materials	Density (kg/m^3)	Young's modulus (MPa)	Poisson's ratio	f_c (MPa)	f_y (MPa)
Concrete	2500	30000	0.2	30	-
Steel	7850	210000	0.3	-	450
EPS	15	6.5	0.12	-	-

Fig. 19 shows the results obtained from the FE analysis simulating the compression test in squat walls. Fig 19a, b show a comparison in terms of crack patterns between the FE analysis and the experimental results relative to the axial compression test in squat walls. It is possible to notice that the majority of (open and partially open) cracks are localized on the top part of the wall, where the experiments highlighted concrete expulsive crushing, below the upper reinforced concrete beam. This failure mechanism is also confirmed in Fig. 19c, d which show an out-of-plane bending phenomenon of the concrete wythes and steel rebars due to the high compressive loads.

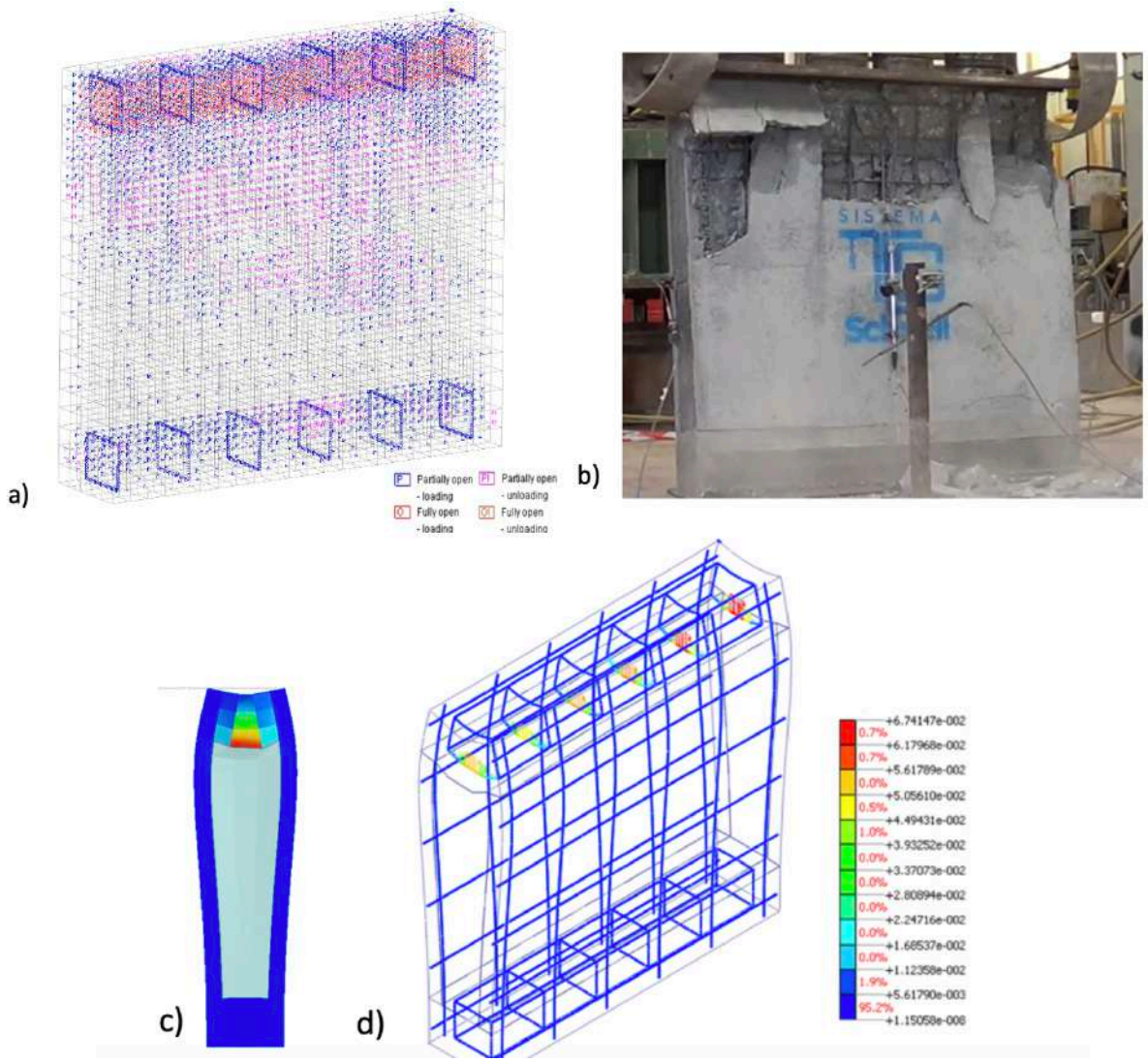

Figure 19. Axial compression test FE analysis: : a) crack pattern (open, partially open and closed cracks), b) experimental crack pattern, c) out-of-plane deformation and d) steel rebars truss equivalent strains map at failure.

In Fig. 20, the load vs vertical displacement graphs obtained from axial compression tests are compared with the results obtained from the FE analysis. The overall trend and the mean initial stiffness of the panels are well-approximated by the numerical model, while a lower agreement is achieved concerning the ultimate compressive load between experiments (mean value = 1541 kN) and numerical simulation (2248 kN). The numerical value was 46% larger than the experimental load. This difference is mainly due to the fact that the behavior of real panels was significantly influenced by geometrical imperfections (not perfectly flat concrete layers, the variability of thicknesses, constraint conditions, etc.) that are difficult to take into consideration in a numerical model. Moreover, the FE model did not take into account the influence of a buckling phenomenon in the RC beam steel rebars, which caused the concrete expulsion and rupture (e.g., Fig. 9a), and loss of compressive capacity.

The numerical curve presents a horizontal plateau at about 1050 kN in correspondence of the steel rebars yielding (see also Fig 18a, b), causing a loss of stiffness of the panel. After yielding, the FE curve starts increasing with a smaller slope, until the ultimate load was reached. It is worth mentioning that, even though the experiments stopped at a lower ultimate load due to concrete crushing, the overall trend, before failure, is well-approximated by the FE simulation: it appears that the experimental curves tend to the numerical one with very similar slopes.

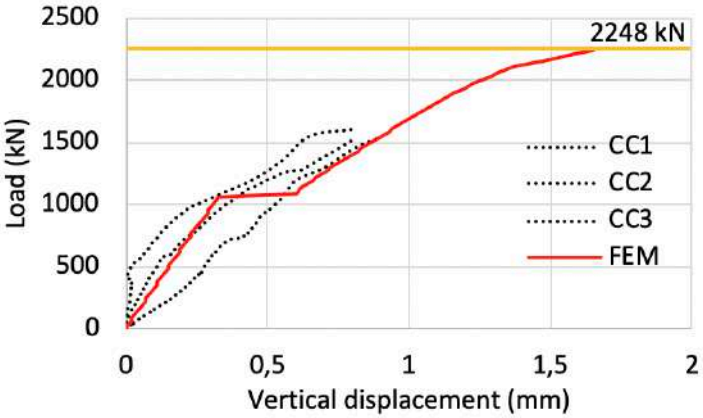

Figure 20. Axial compression test: comparison between experimental and numerical results.

Fig. 21 shows the results obtained from the FE analysis simulating the diagonal compression tests. As shown in Fig. 21a,b, the cracks are concentrated on the top or bottom corners, corresponding to the localized concrete crushing. This is also confirmed by the concentration of out-of-plane deformations and maximum equivalent strains for the concrete layers and steel rebars and mesh at the loading application points (Fig. 21 c,d).

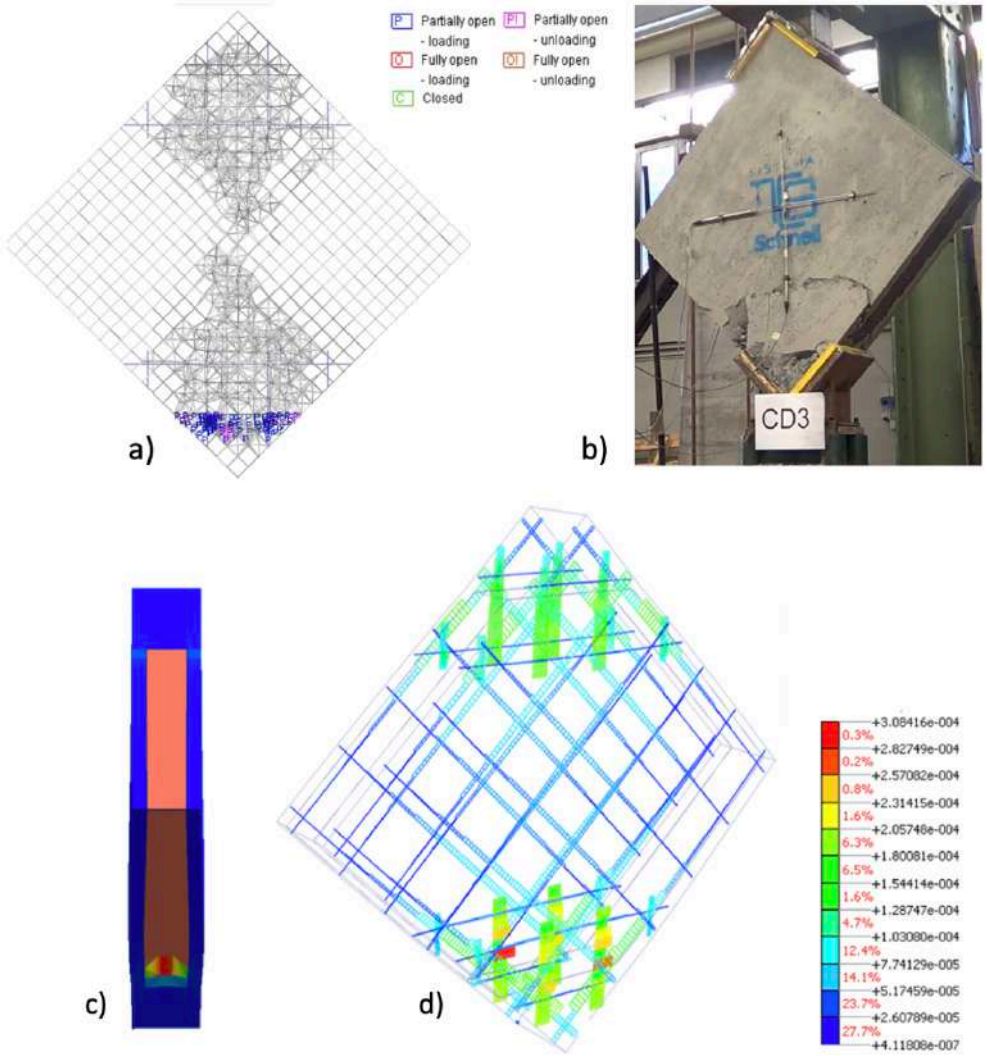

Figure 21. Diagonal compression test FE analysis: : a) crack pattern (open, partially open and closed cracks), b) experimental crack pattern, c) out-of-plane deformation and d) steel rebars truss equivalent strains map at failure.

In Fig. 22 the load-vertical displacement plot experimentally obtained is compared with the results obtained with the numerical model. The mechanical behavior of the specimen was linear elastic till failure. The overall trend was well-simulated by the model and the numerical value of the ultimate load (407 kN) was close to the mean experimental value (446 kN), with a difference of 9%.

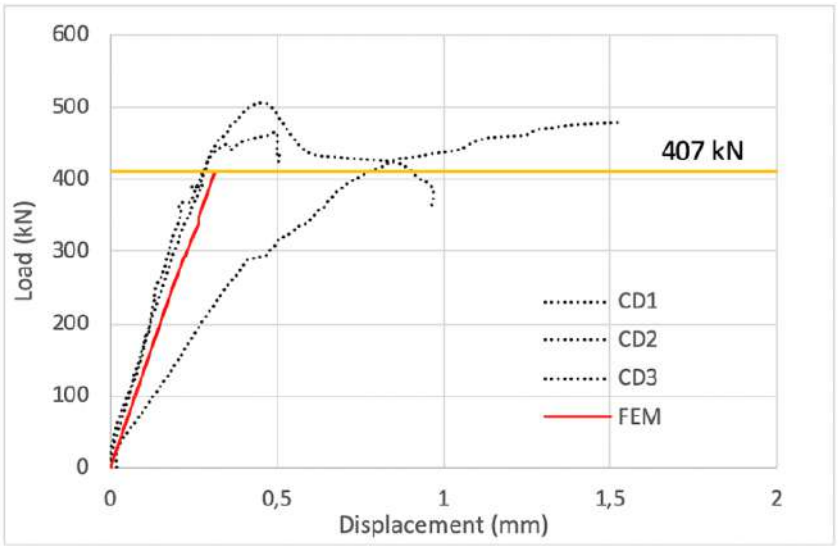

Figure 22. Diagonal compression test: comparison between experimental and numerical results.

In Fig. 23 the results, obtained from the FE analysis on the shear test, are reported. Figures 23a,b,c,d show the plots of the crack pattern, the Von Mises equivalent strain and the steel rebar truss equivalent strains at failure. It is possible to notice that the concentration of the strain (and, hence, stresses) are localized in the bottom corner regions, opposite to the top loading edge, where the concrete presented an expulsive crushing. The Von Mises plot also shows the formation of the typical diagonal compression strut, orthogonal to the main diagonal cracks. Moreover, the crack pattern of the panel reported a concentration of open and partially open cracks on the bottom edge region.

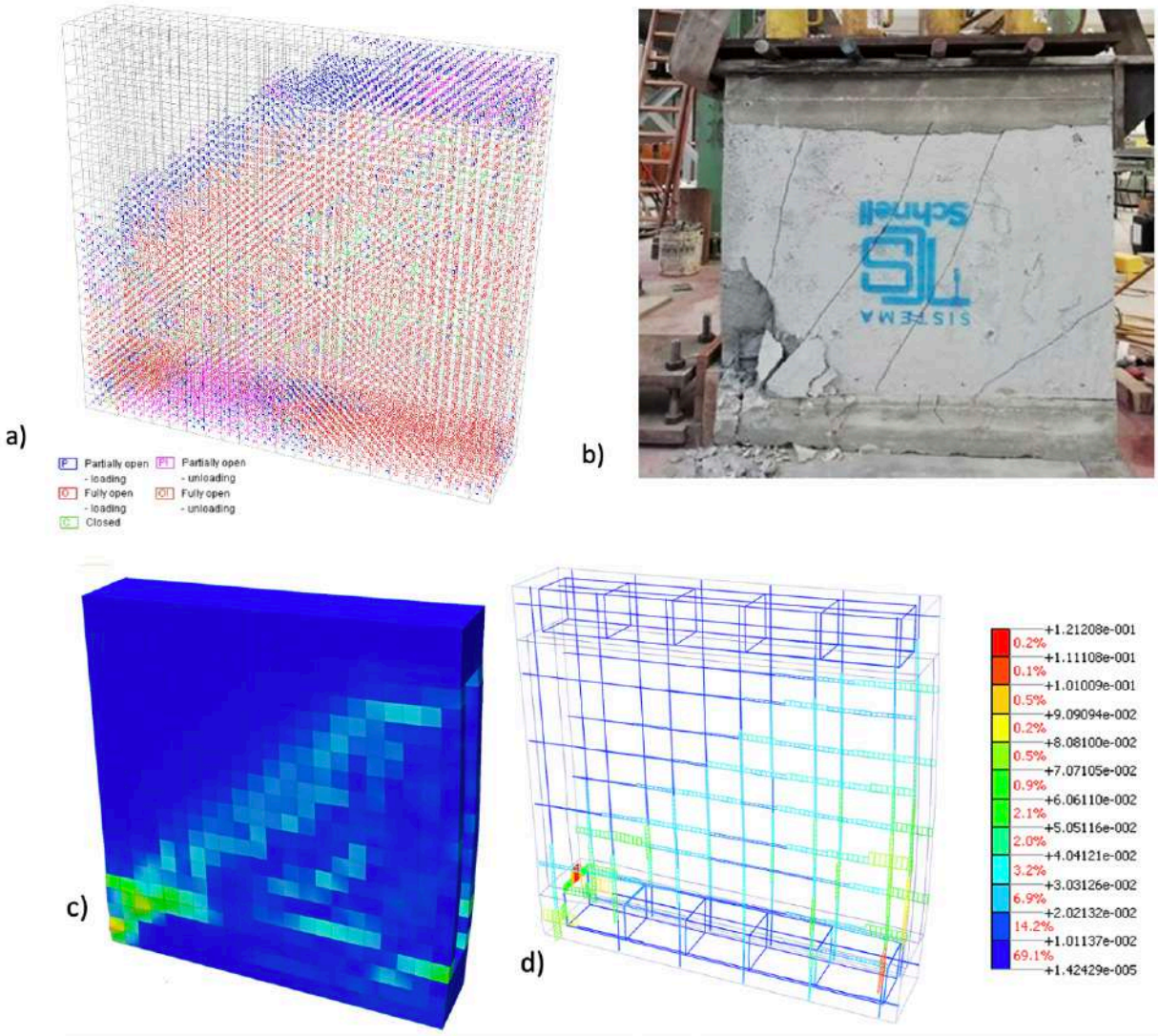

Figure 23. Shear test with compression FE analysis: a) crack pattern (open, partially open and closed cracks), b) experimental crack pattern, c) out-of-plane deformation and d) steel rebars truss equivalent strains map at failure.

Finally, Fig. 24 represents the comparison in terms of applied horizontal load versus drift between the experimental and numerical results. Even though the FE model appeared to be initially stiffer than the experimental counterpart, a good agreement in terms of ultimate shear strength was achieved with a 3% difference between the FE analysis (263 kN) and the experimental campaign (256 kN).

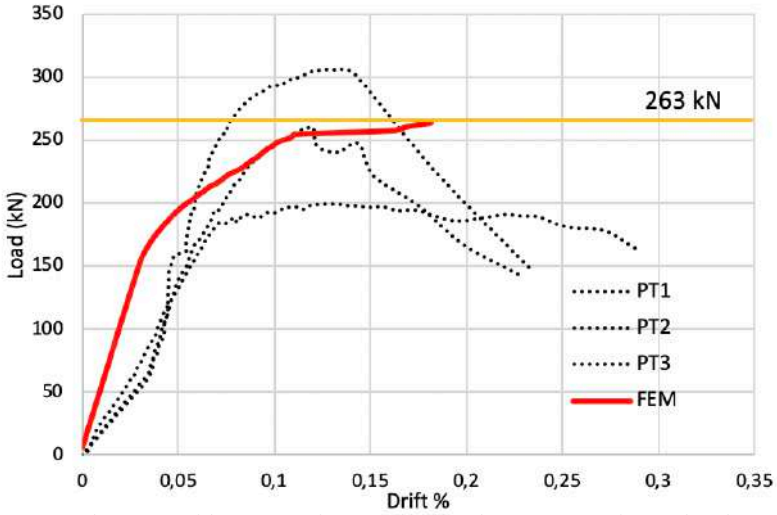

Figure 24. Shear test with compression: comparison between experimental and numerical results.

5. Conclusions

The present research paper focuses on the experimental and numerical characterization of the in-plane and shear behaviors of sprayed in-situ RC sandwich panels. In particular, the experimental campaign consisted of axial compression, diagonal compression, and horizontal shear with compression tests. The experiments have been compared with a numerical 3D nonlinear FE model, taking into account the presence of the insulation layer, the efficiency of steel connectors in the composite action, and the involved material nonlinearities.

High ultimate loads (Table 3), decreasing for increasing slenderness ratios, have been obtained from axial compression tests. The attained high values (about 1500 kN), the low values of the maximum relative separation displacements between the two concrete wythes (about 0.8 mm) as well as the presence of the two top and bottom RC beams confirmed that the RC sandwich walls showed a partially composite behavior. The experimental axial tests may be representative of real buildings in which the connections between floor and wall panels are built with solid reinforced concrete regions. The above results proved the structural potentialities of RC sandwich panels as load-bearing walls. Moreover, the use of sprayed concrete proved to be efficient with no evident splitting from the EPS substrate. Finally, the nonlinear FE analysis well-approximated the overall trend under axial compression, identifying the regions in which the main failure due to concrete crushing has arisen, even though the numerical value of the ultimate load (2248 kN) was 46 % higher than the experimental value (1555 kN). This could be justified by the real non-uniform load distribution within the concrete layers, due to undesired eccentricities, which resulted in premature experimental failure and loss of compressive capacity.

The shear tests (diagonal compression and shear test with constant compression) results showed a high capacity for stress redistribution thanks to the metallic mesh inside the concrete layers, providing a semi-composite behavior till rupture. The main failure mechanism was similar to classical masonry or RC walls and was represented by the formation of the typical diagonal cracks and a relevant concrete spalling on the corner of the load application point. The experimental results have been confirmed by the numerical simulations of both diagonal compression and shear test in terms of ultimate tensile load and crack patterns. The shear capacity of RC sandwich panels under horizontal forces can be considered comparable with the lateral performance of conventional RC walls, having similar geometric and mechanical properties. However, since the shear behavior is significantly influenced by the dimensions of the wall, the presence of openings, and reinforced concrete boundary elements, further experimental and numerical investigations on RC sandwich panels are strongly required.

Acknowledgments

The financial support provided by TCS S.r.l., that provides the tested panels, is gratefully acknowledged. The technical support of Andrea Conti, Franco Rinaldi and Elisa Cartechini of the Dept. of Civil and Building Engineering, and Architecture, Università Politecnica delle Marche, has been greatly appreciated. The opinions, findings and conclusions contained in this paper are those of the authors, and do not necessarily reflect the views of the sponsors.

References

[1] E. D. Losch *et al.*, “State of the art of precast/prestressed concrete sandwich wall panels,” *PCI J.*, 2011.

[2] G. Woltman, M. Noel, and A. Fam, “Experimental and numerical investigations of thermal properties of insulated concrete sandwich panels with fiberglass shear connectors,” *Energy Build.*, vol. 145, pp. 22–31, Jun. 2017.

[3] A. Jawdhari and A. Fam, “Thermal-Structural Analysis and Thermal Bowing of Double Wythe UHPC Insulated Walls,” *Energy Build.*, vol. 223, p. 110012, Sep. 2020.

[4] S. Suryani and N. Mohamad, “Structural Behaviour of Precast Lightweight Foamed Concrete Sandwich Panel under Axial Load : An Overview,” *Int. J. Integr. Eng.*, 2012.
[5] M. Serpilli and S. Lenci, “An overview of different asymptotic models for anisotropic three-layer plates with soft adhesive,” *Int. J. Solids Struct.*, vol. 81, 2016.
[6] R. O’Hegarty and O. Kinnane, “Review of precast concrete sandwich panels and their innovations,” *Constr. Build. Mater.*, vol. 233, p. 117145, Feb. 2020.
[7] A. Benayoune, A. A. A. Samad, D. N. Trikha, A. A. Abang Ali, and A. A. Ashrabov, “Structural behaviour of eccentrically loaded precast sandwich panels,” *Constr. Build. Mater.*, vol. 20, no. 9, pp. 713–724, Nov. 2006.
[8] A. Benayoune, A. A. A. Samad, A. A. Abang Ali, and D. N. Trikha, “Response of pre-cast reinforced composite sandwich panels to axial loading,” *Constr. Build. Mater.*, vol. 21, no. 3, pp. 677–685, Mar. 2007.
[9] F. Gara, L. Ragni, D. Roia, and L. Dezi, “Experimental tests and numerical modelling of wall sandwich panels,” *Eng. Struct.*, vol. 37, pp. 193–204, Apr. 2012.
[10] Y. H. Mugahed Amran, A. A. Abang Ali, R. S. M. Rashid, F. Hejazi, and N. A. Safiee, “Structural behavior of axially loaded precast foamed concrete sandwich panels,” *Constr. Build. Mater.*, vol. 107, pp. 307–320, Mar. 2016.
[11] Y. H. Mugahed Amran, R. Alyousef, H. Alabduljabbar, F. Alrshoudi, and R. S. M. Rashid, “Influence of slenderness ratio on the structural performance of lightweight foam concrete composite panel,” *Case Stud. Constr. Mater.*, vol. 10, p. e00226, Jun. 2019.
[12] L. Graziani, E. Quagliarini, M. D’Orazio, S. Lenci, and A. Scalbi, “A More Sustainable Way for Producing RC Sandwich Panels On-Site and in Developing Countries,” *Sustainability*, vol. 9, no. 3, p. 472, Mar. 2017.
[13] D. Tomlinson and A. Fam, “Analysis and Parametric Study of Partially Composite Precast Concrete Sandwich Panels under Axial Loads,” *J. Struct. Eng.*, vol. 142, no. 10, p. 04016086, Oct. 2016.
[14] Q. Huang, E. Hamed, and R. I. Gilbert, “Behavior of Concrete Sandwich Panels under Eccentric Axial Compression—Testing and Finite Element Analysis,” *ACI Struct. J.*, 2020.
[15] J. Daniel Ronald Joseph, J. Prabakar, and P. Alagusundaramoorthy, “Experimental study on the behavior of lightweight concrete sandwich panels under axial compression,” *J. Struct. Eng.*, vol. 44, no. 6, pp. 568–576, 2018.
[16] P. M. Hopkins, A. Chen, and M. Yossef, “Static and dynamic analyses of insulated concrete sandwich panels using a unified non-linear finite element model,” *Eng. Struct.*, vol. 132, pp. 249–259, Feb. 2017.
[17] M. Z. Kabir, “Structural performance of 3-D sandwich panels under shear and flexural loading,” *Sci. Iran.*, 2005.
[18] I. Ricci, M. Palermo, G. Gasparini, S. Silvestri, and T. Trombetti, “Results of pseudo-static tests with cyclic horizontal load on cast in situ sandwich squat concrete walls,” *Eng. Struct.*, vol. 54, pp. 131–149, Sep. 2013.
[19] A. Pavese and D. A. Bournas, “Experimental assessment of the seismic performance of a prefabricated concrete structural wall system,” *Eng. Struct.*, 2011.
[20] M. Palermo and T. Trombetti, “Experimentally-validated modelling of thin RC sandwich walls subjected to seismic loads,” *Eng. Struct.*, 2016.
[21] E. Brunesi, R. Nascimbene, and A. Pavese, “Mechanical model for seismic response assessment of lightly reinforced concrete walls,” *Earthq. Struct.*, 2016.
[22] F. A. I. Refaei, M. T. El-Mihilmy, and T. M. Bahaa, “Seismic Behavior of Sandwich Panel Walls,” *World Appl. Sci. J.*, 2015.
[23] A. Wibowo, I. Wijatmiko, and C. R. Nainggolan, “Cyclic Behaviour of Expanded Polystyrene (EPS) Sandwich Reinforced Concrete Walls,” *Adv. Mater. Sci. Eng.*, vol. 2018, pp. 1–9, Dec. 2018.
[24] W. Qiao, X. Yin, S. Zhao, and D. Wang, “Cyclic loading test study on a new cast-in-situ

insulated sandwich concrete wall," *PLoS One*, vol. 14, no. 11, p. e0225055, Nov. 2019.
[25] E. Brunesi, S. Peloso, R. Pinho, and R. Nascimbene, "Cyclic testing and analysis of a full-scale cast-in-place reinforced concrete wall-slab-wall structure," *Bull. Earthq. Eng.*, vol. 16, no. 10, pp. 4761–4796, Oct. 2018.
[26] A. Benayoune, A. A. A. Samad, D. N. Trikha, A. A. A. Ali, and S. H. M. Ellinna, "Flexural behaviour of pre-cast concrete sandwich composite panel – Experimental and theoretical investigations," *Constr. Build. Mater.*, vol. 22, no. 4, pp. 580–592, Apr. 2008.
[27] J. Daniel Ronald Joseph, J. Prabakar, and P. Alagusundaramoorthy, "Flexural behavior of precast concrete sandwich panels under different loading conditions such as punching and bending," *Alexandria Eng. J.*, vol. 57, no. 1, pp. 309–320, Mar. 2018.
[28] G. Carbonari, S. H. P. Cavalaro, M. M. Cansario, and A. Aguado, "Flexural behaviour of light-weight sandwich panels composed by concrete and EPS," *Constr. Build. Mater.*, vol. 35, pp. 792–799, Oct. 2012.
[29] A. Chen, T. G. Norris, P. M. Hopkins, and M. Yossef, "Experimental investigation and finite element analysis of flexural behavior of insulated concrete sandwich panels with FRP plate shear connectors," *Eng. Struct.*, vol. 98, pp. 95–108, Sep. 2015.
[30] D. Dutta, A. Jawdhari, and A. Fam, "A New Studded Precast Concrete Sandwich Wall with Embedded Glass-Fiber-Reinforced Polymer Channel Sections: Part 1, Experimental Study," *PCI J.*, vol. 65, no. 3, 2020.
[31] A. Jawdhari and A. Fam, "A New Studded Precast Concrete Sandwich Wall with Embedded Glass-Fiber-Reinforced Polymer Channel Sections: Part 2, Finite Element Analysis and Parametric Studies," *PCI J.*, vol. 65, no. 4, 2020.
[32] D. Tomlinson and A. Fam, "Flexural behavior of precast concrete sandwich wall panels with basalt FRP and steel reinforcement," *PCI Journal*. 2015.
[33] D. Tomlinson and A. Fam, "Analytical approach to flexural response of partially composite insulated concrete sandwich walls used for cladding," *Eng. Struct.*, vol. 122, pp. 251–266, Sep. 2016.
[34] H. Hou, W. Wang, B. Qu, and C. Dai, "Testing of insulated sandwich panels with GFRP shear connectors," *Eng. Struct.*, vol. 209, p. 109954, Apr. 2020.
[35] ASTM E519/E519M-15, "Standard Test Method for Diagonal Tension (Shear) in Masonry Assemblages," *ASTM Int. West Conshohocken, PA*, 2015.
[36] E. Quagliarini, S. Lenci, and M. Iorio, "Mechanical properties of adobe walls in a Roman Republican domus at Suasa," *J. Cult. Herit.*, vol. 11, no. 2, pp. 130–137, Apr. 2010.
[37] F. Stazi, M. Serpilli, G. Chiappini, M. Pergolini, E. Fratalocchi, and S. Lenci, "Experimental study of the mechanical behaviour of a new extruded earth block masonry," *Constr. Build. Mater.*, vol. 244, p. 118368, May 2020.
[38] M. S. Saheb and P. Desayi, "Ultimate strength of R.C. wall panels in two-way in-plane action," *J. Struct. Eng. New York, N.Y.*, 1990.
[39] ACI Committee 318, "ACI 318-14," *Build. Code Requir. Struct. Concr.*, 2014.
[40] M. Frocht, "Recent advances in photoelasticity," *ASME Trans*, 1931.
[41] Eurocode 8, *Design of structures for earthquake resistance*. 2005.
[42] A. Sánchez-Alejandre and S. M. Alcocer, "Shear strength of squat reinforced concrete walls subjected to earthquake loading — trends and models," *Eng. Struct.*, vol. 32, no. 8, pp. 2466–2476, Aug. 2010.
[43] J. Carrillo and S. M. Alcocer, "Shear strength of reinforced concrete walls for seismic design of low-rise housing," *ACI Struct. J.*, 2013.
[44] C. Kerem Gulec and A. S. Whittaker, "Empirical equations for peak shear strength of low aspect ratio reinforced concrete walls," *ACI Struct. J.*, 2011.
[45] F. Clementi, V. Gazzani, M. Poiani, P. A. Mezzapelle, and S. Lenci, "Seismic Assessment of a Monumental Building through Nonlinear Analyses of a 3D Solid Model," *J. Earthq. Eng.*, vol. 22, no. sup1, pp. 35–61, Sep. 2018.